Supplementary Materials for

Programmable and reversible assembly of soft capillary multipoles

Jinhye Bae, Nakul P. Bende, Arthur A. Evans, Jun-Hee Na, Christian D. Santangelo,* Ryan C. Hayward*

*Corresponding author. E-mail: csantang@physics.umass.edu (C.D.S.); hayward@umass.edu (R.C.H.)

This PDF file includes:

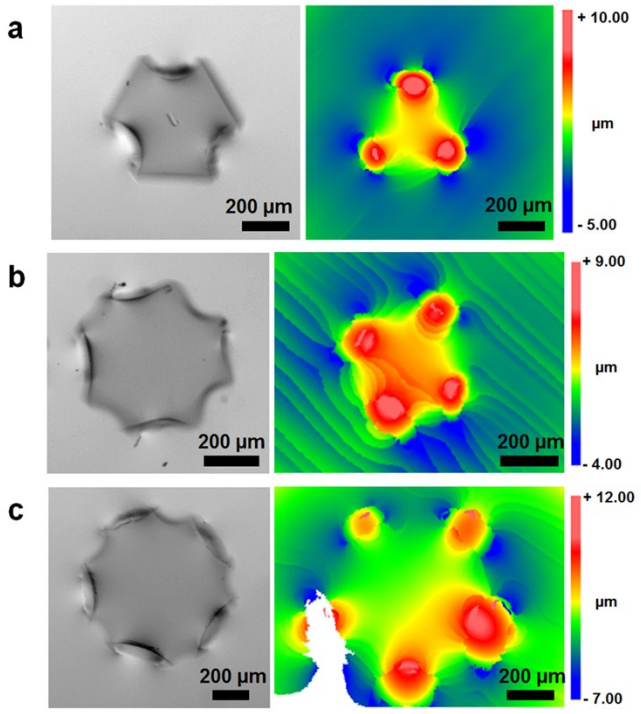

Fig. S1. Interface deformation by isometic deformation of Enneper's minimal surfaces. Optical micrographs (left) and profilometry images (right) of swelled SPGP with n = (**a**) 3, (**b**) 4 and (**c**) 5 at the air/water interface. The inverted "J" in the center of the SPGP shown in (**a**) indicates that the SPGP is 'up-side down', and therefore that the splitting of troughs seen in both orientations (see Fig. 2a of the main text for the 'right-side up' case) represents a symmetry breaking driven by adsorption at the interface, rather than an inherent up/down asymmetry in the shape of the particle.

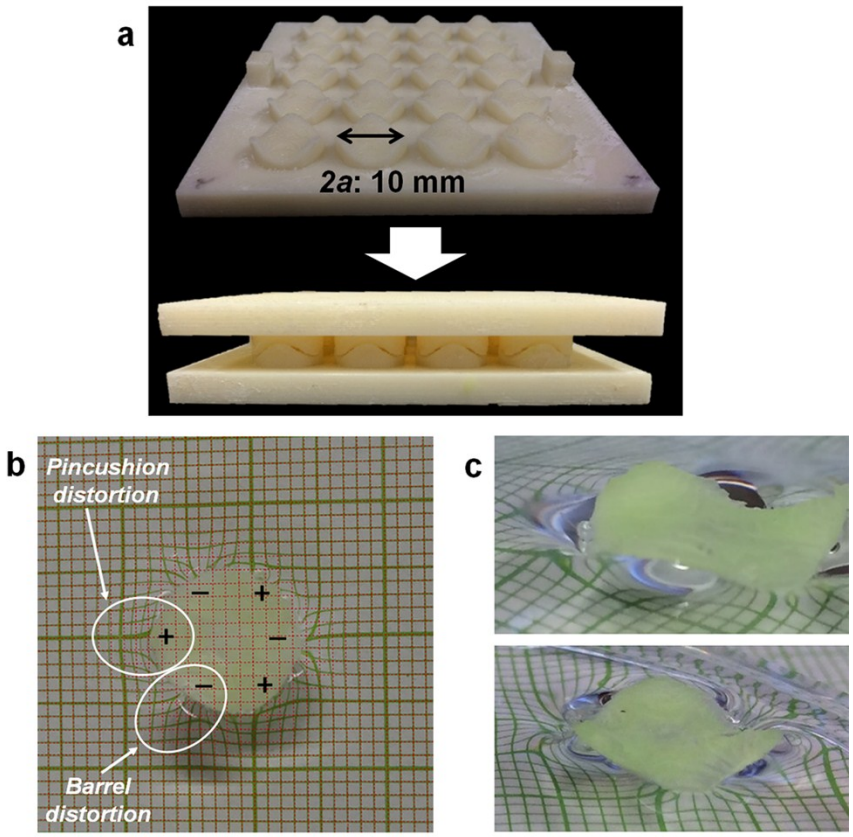

Fig. S2. Fabrication and interfacial adsorption of elastomer particles. (**a**) An array of 3D printed two sided molds used to fabricate elastomer particles with $n = 3$. Photographs showing (**b**) top and (**c**) side views of the hexapolar interfacial deformation induced by adsorption of elastomer particles at the air/water interface. (**b**) The alternation between similar magnitude 'pincushion' distortions at the crests and 'barrel' distortions at the troughs (seen by comparing the positions of the green lines on the underlying grid to the orthoscopic case of a flat interface, as indicated by the red dotted lines) reveals that the particle does not deform appreciably upon adsorbing to the interface.

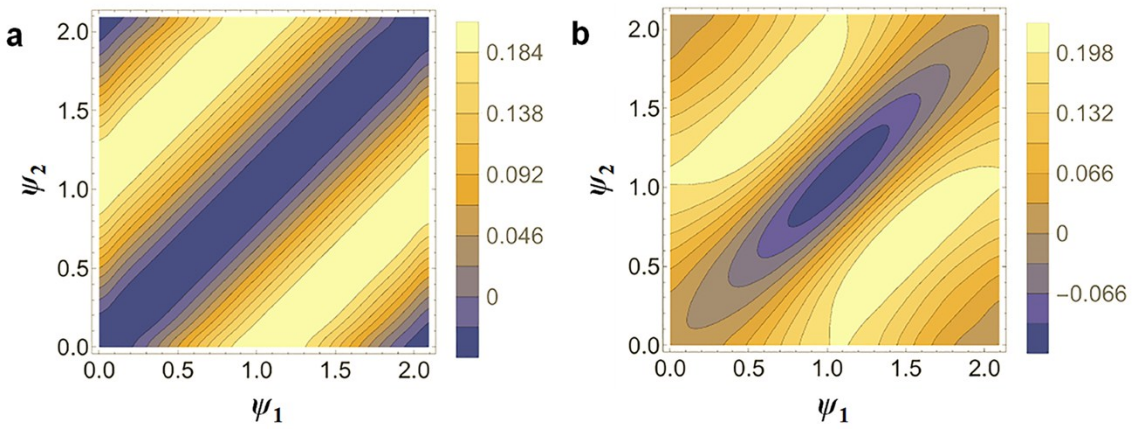

Fig. S3. Energy landscape for two capillary multipoles. (**a**) The capillary energy landscape as a function of orientation angle for two purely hexapolar particles, and (**b**) for two particles consisting of a hexapole and a dodecapole (with amplitude ratios of 1 : 0.5). In the former case, the minimum energy occurs for any value of $\psi_1 = \psi_2$, while in the latter case a unique minimum exists at $\psi_1 = \psi_2 = \pi/3$. For reasons of symmetry, we plot ψ only from 0 to $2\pi/n$. The color scale indicates the multipolar interaction energy normalized by γH^2, where H is the hexapole amplitude.

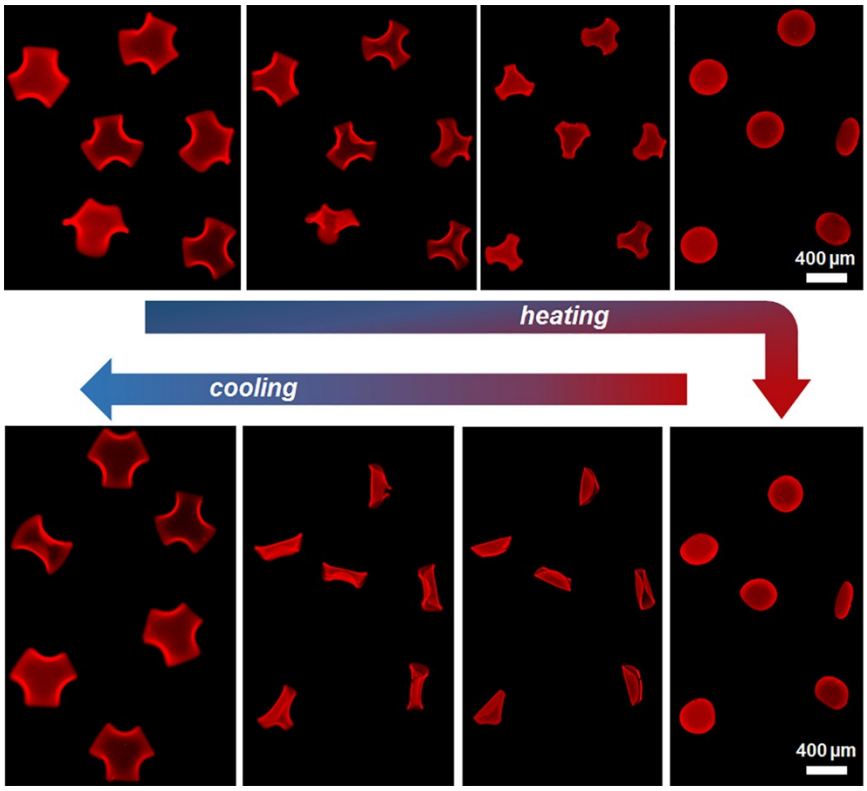

Fig. S4. Thermally-controlled deformation of non-adsorbed SPGPs. Upon heating, non-interfacially-adsorbed 3-node SPGPs deswell and recover their flat shape by 54 °C, while upon cooling, the flat disks swell back to their programmed shapes by 25 °C.

I. Isometric deformations of an elastic Enneper's surface

The elastomeric particles are shells with a preferred curvature, while the SPGPs are non-Euclidean disks that take on the shape of Enneper's surface in response to in-plane residual stresses. In both cases, the dominant mechanical deformations arise purely from bending of the surface, since stretching is energetically costly. Defining the surface by a parametrization **X**(u,v), where *u* and *v* are internal variables local to the surface itself, for Enneper's minimal surface with k crests we have

$$X(u,\upsilon;k)=\left\{u\cos\upsilon-\frac{u^{2k-1}}{2k-1}\cos(2k-1)\upsilon, u\sin\upsilon+\frac{u^{2k-1}}{2k-1}\sin(2k-1)\upsilon, \frac{2u^{k}}{k}\cos k\upsilon\right\} \tag{1}$$

From here we calculate the metric and curvature tensors, $g_{\alpha\beta}$ and $d_{\alpha\beta}$, respectively, to determine the elastic energy content of the surface under small deformations. Within the framework of linear elasticity the energy density of deformation may be written as

$$W=\frac{Yh}{2(1-v^2)}\left[\left\{(1-v)E^{\alpha}_{\beta}E^{\beta}_{\alpha}+vE^{\alpha}_{\alpha}E^{\beta}_{\beta}\right\}+\frac{h^2}{12}\left\{(1-v)K^{\alpha}_{\beta}K^{\beta}_{\alpha}+vK^{\alpha}_{\alpha}K^{\beta}_{\beta}\right\}\right], \tag{2}$$

where *Y* is Young's modulus, *v* Poisson's ratio, and *h* the thickness. We have also defined the strain and bending tensors $E_{\alpha\beta}=\frac{1}{2}(g^{*}_{\alpha\beta}-g_{\alpha\beta})$ and $K_{\alpha\beta}=d^{*}_{\alpha\beta}-d_{\alpha\beta}$, respectively, where the starred tensor refers to the deformed surface.

A. Diffuse isometries

For a displacement of the surface of the form $X + \varepsilon_u T_u + \varepsilon_\upsilon T_\upsilon + \zeta \hat{n}$, where T_i is the tangent vector on the surface in the i^{th} direction and $\hat{n}$ is the local normal vector, we may write the linearized strain tensor as

$$E_{\alpha\beta} = \frac{1}{2}\left(D_\alpha \varepsilon_\beta + D_\beta \varepsilon_\alpha\right) - d_{\alpha\beta}\zeta\,, \tag{3}$$

With D_i the covariant derivative defined on the surface.

Based on estimates of the elasto-capillary stretching and bending numbers (see main text), it is unlikely that any stretching will occur, but surface tension may be responsible for bending the surfaces. For a stretch-free surface, the deformations are necessarily strain-free as well (isometries of the surface). These deformations to linear order in the displacements are given by

$$E_{uu} = D_u \varepsilon_u - d_{uu}\zeta = 0\,, \tag{4}$$

$$E_{u\upsilon} = D_u \varepsilon_\upsilon + D_\upsilon \varepsilon_u - 2d_{u\upsilon}\zeta = 0\,, \tag{5}$$

$$E_{\upsilon\upsilon} = D_\upsilon \varepsilon_\upsilon - d_{\upsilon\upsilon}\zeta = 0\,, \tag{6}$$

The normal deflection ζ may be eliminated in favor of the other two displacements, yielding equations for ε_u and ε_υ. Assuming that these displacements have the same azimuthal symmetry as the reference curvature, we let $\varepsilon_u = A(u)\cos k\upsilon$ and $\varepsilon_\upsilon = B(u)\sin k\upsilon$, which allows for the amplitudes *A*, *B* to be found analytically. For example, with $k = 3$:

$$A(u) = C_1 u^3 + C_2\left(u^5 + \frac{6}{5}u^9 + \frac{13}{25}u^{13}\right), \tag{7}$$

$$B(u) = -C_1 u^2 - C_2\left(\frac{3}{5}u^4 + \frac{2}{5}u^8 + \frac{3}{25}u^{12}\right), \tag{8}$$

where C_i are integration constants that depend on the imposed boundary conditions at the edge of the sheet. From this we may calculate the first order isometric deformations and see how they alter the capillary signature of the gel sheet. See Fig. 1i for an example of the isometry given by boundary conditions $A(1) = 0$, $B(1) = 1$, corresponding to pure tangential stretching of the surface. The isometric deformations naturally break the symmetry of the reference state, and the crest/trough asymmetry seen in experiments can be explained since the gel Enneper's surface is driven to the interface from within the bulk, or by the preferred contact angle at the particle/air/water interface.

II. Capillary multipoles: Two disks

For objects much smaller than the capillary length, $\nabla^2 h = (1/l_c)^2 h$ (where h is the height and l_c is the capillary length) reduces to $\nabla^2 h = 0$, which we can solve exactly for two disks. The derivation is as follows[1-3]:

We consider two shapes whose projected contact lines are disks of radius R whose centers are separated by a distance d. This system may be solved exactly over distances $L << l_c$, so that we effectively just need to solve Laplace's equation with Dirichlet data. We change to bipolar coordinates, such that

$$x = \alpha \frac{\sinh\eta}{\cosh\eta - \cos\xi}, \tag{9}$$

$$y = \alpha \frac{\sinh\zeta}{\cosh\eta - \cos\xi}, \tag{10}$$

Where $\alpha = (d/2 - R)(d/2 + R)$. The surfaces of the disks are given by surfaces of constant $\eta = \eta_0 = \cosh^{-1}(d/2R)$, where $\eta_A = -\eta_0 = -\eta_B$ for particles A and B, respectively. In these coordinates, Laplace's equation is given by $\left(\partial_\eta^2 + \partial_\varepsilon^2\right)h = 0$, for which we can give $h(\eta, \xi)$ in terms of a Fourier expansion:

$$h(\eta,\xi) = H_A \sum_n (C_n \cos n\xi + D_n \sin n\xi) \frac{\sinh n(\eta_A + \eta)}{\sinh n(\eta_A + \eta_B)} + H_B \sum_n (E_n \cos n\xi + F_n \sin n\xi) \frac{\sinh n(\eta_B - \eta)}{\sinh n(\eta_A + \eta_B)} \tag{11}$$

For the case of identical disks with a single multipole of degree *m*, the contact line height for particle A is given by $\cos m(\phi - \phi_A)$, we solve for these unknown coefficients in terms of infinite series, and thus find the height field everywhere. We also calculate the change in the surface area and thus derive an interaction energy between the disks; this is given by

$$E_{AB,m} = H_A^2 S_A + H_B^2 S_B - H_A H_B G \cos m(\phi_A - \phi_B), \tag{12}$$

$$S_j = \sum_{n=1}^{\infty} \frac{n}{2} \coth n(\eta_A + \eta_B) A^2(n, m, \eta_j), \tag{13}$$

$$G = \sum_{n=1}^{\infty} \frac{A(n, m, \eta_A) A(n, m, \eta_B)}{\sinh n(\eta_A + \eta_B)}, \tag{14}$$

$$A(n, m, \eta_j) = m \sum_{k=0}^{\min(m,n)} \frac{(-1)^{m-ki} (m + n - k - 1)!}{(m-k)!(n-k)!k!} e^{-(m+n-2k)\eta_j}, \tag{15}$$

Elastocapillary interactions break the symmetry of the Enneper's disks, and thus introduce a higher order multipole into the system. This additional interaction energy breaks the degeneracy of the single multipole energy and leads to a well-defined minimum.

A. Two-body interactions

This approximation works well for the gel system. For the elastomer Enneper shells we must resort to the superposition approximation, but in both cases there is a pair potential that takes the form $U(r;n,m)\cos(n\phi_1 - m\phi_2)$, where the function $U(r;n,m)$ decays with increasing distance r between the particles, and *n*,*m* are the capillary multipole moments for the particles. In the case of the gel sheets, the pair potential in the superposition approximation has the simple power law form $U(r) \sim 1/r^{2n}$, with the full form given by the analytical series expansion given in the supplement Eq. (12-15). For the elastomer shells, the length scales involved are larger than the capillary length, and thus the forces involved are not simple power laws.

Movie S1. A movie showing interfacial pairing of 3-node SPGPs at the air/water interface. The center-to-center separation distance (*L*) relative to body length (*2a* = 640 μm) and the difference in orientation angle $\Delta\psi$ were tracked as a function of time until contact.

Movie S2. A real time movie showing assembly of two trimers of 3-node SPGPs ($2a$ = 640 μm) into an open hexagonal structure at the air/water interface (imaging area: 4.4 mm x 3.3 mm).

Movie S3. A real time movie showing frustrated assembly of 3-node SPGPs ($2a$ = 640 μm) into a square structure (imaging area: 4.4 mm x 3.3 mm).

Movie S4. A movie (2x real speed) showing assembly of 5-node elastomer particles ($2a$ = 10 mm) at the air/water interface.

Movie S5. A movie showing thermally switchable capillary assembly of 3-node SPGPs at the air/water interface.

References

1 Kralchevsky, P. A., Denkov, N. D. & Danov, K. D. Particles with an Undulated Contact Line at a Fluid Interface: Interaction between Capillary Quadrupoles and Rheology of Particulate Monolayers. *Langmuir* **17**, 7694-7705 (2001).

2 Danov, K. D., Kralchevsky, P. A., Naydenov, B. N. & Brenn, G. Interactions between particles with an undulated contact line at a fluid interface: Capillary multipoles of arbitrary order. *J. Colloid Interface Sci.* **287**, 121-134 (2005).

3 Danov, K. D. & Kralchevsky, P. A. Capillary forces between particles at a liquid interface: General theoretical approach and interactions between capillary multipoles. *Adv. Colloid Interface Sci.* **154**, 91-103 (2010).